GEOPHYSICAL RESEARCH LETTERS, VOL. 36, L10702, doi:10.1029/2009GL038259, 2009

Present and future atmospheric blocking and its impact on European mean and extreme climate

Jana Sillmann[1] and Mischa Croci-Maspoli[2]

Received 25 March 2009; accepted 22 April 2009; published 20 May 2009.

[1] Atmospheric blocking plays an important role in the mid-latitude climate variability and can be responsible for anomalous mean and/or extreme climate. In this study, a potential vorticity based blocking indicator is used to investigate the representation of Euro-Atlantic atmospheric blocking events in the ECHAM5/MPI-OM climate model. The impact of blocking events on present and future mean and extreme climate is studied by means of composite maps and correlation analyses. In comparison to ERA-40 reanalysis, the model represents the blocking frequency and seasonal distribution well. We show that European blocking events have a sustained influence particularly on anomalous cold winter temperatures in Europe. In a future climate, the blocking frequency is slightly diminished but the influence on the European winter climate remains robust. Due to a northeastward shift of the blocking pattern and an increase in maximum blocking duration, cold winter temperature extremes can still be expected in a future climate. **Citation:** Sillmann, J., and M. Croci-Maspoli (2009), Present and future atmospheric blocking and its impact on European mean and extreme climate, *Geophys. Res. Lett.*, *36*, L10702, doi:10.1029/2009GL038259.

1. Introduction

[2] For a better understanding and improved prediction of changes in the mean and extreme climate it is of major importance to investigate their link to large-scale circulation patterns. In this respect atmospheric blocking (anti-cyclonic quasi-stationary high-pressure system persisting for several days up to weeks) acts as a prominent feature with considerable impacts on the Euro-Atlantic climate. Atmospheric blocking plays a key role in the European flow variability due to its capability to disturb the predominant cyclonic westerly flow. Owing to its large spatial extent and temporal persistence, it can be responsible for e.g. dry and cold winters at its core and downstream of the block and wet conditions around the block [e.g., *Trigo et al.*, 2004] (hereinafter referred to as T04).

[3] Several studies in the past have pointed to the lacking accuracy of General Circulation Models (GCM's) to represent atmospheric blocking, particularly in the Euro-Atlantic region [e.g., *Tibaldi and Molteni*, 1990, hereinafter referred to as TM90; *D'Andrea et al.*, 1998; *Doblas-Reyes et al.*, 2002; *Pelly and Hoskins*, 2003]. Thus, we first investigate how well Euro-Atlantic blocks, represented by a Potential Vorticity (PV)-based blocking indicator, are simulated in the coupled atmosphere-ocean model ECHAM5/MPI-OM.

[4] We further analyze variables such as the 500 hPa geopotential height, surface temperature and precipitation during blocking events close to the European continent under present and future climate conditions to illustrate their impact on the mean European climate. We finally investigate the associations of these blocking events to extreme climate events by correlating them with monthly indices for extreme precipitation and temperature.

2. Data and Methodologies

2.1. Model Experiments

[5] In this study the climate model ECHAM5/MPI-OM (T63/L31) [*Jungclaus et al.*, 2006] is employed, hereinafter referred to as ECHAM5. The model does not employ flux adjustments. Greenhouse gases (GHG) and sulfate aerosols in the 20th century simulations (20C) are prescribed according to observations and chemical transport model results, respectively. For the analysis of the present-day climate (time period 1961–2000), we use 6-hourly data generated from the 20C simulations consisting of a three-member ensemble. We compare the 20C results with ERA-40 reanalysis data (ERA-40 hereinafter) [*Uppala et al.*, 2005]. The analysis of the future climate is based on 6-hourly data generated from a three-member ensemble simulation of the IPCC SRES scenario A1B. To avoid major trends in the time series, we use the last 40 years (2160–2199) of the stabilization period (GHG and aerosol concentrations kept constant at the level of year 2100), where the climate simulations have reached quasi-stable conditions. We concentrate our analyses on the winter (December to February, DJF) and summer season (June to August, JJA).

2.2. Blocking Indicator

[6] In the last decades several attempts have been undertaken to objectively define atmospheric blocking events. They all tie in with the common characteristics of blocking such as enhanced sea level pressure, elevated geopotential height or anticyclonic wind field. The 500 hPa geopotential height (Z500) has been a widely used base field for blocking indicators [e.g., TM90; *Dole and Gordon*, 1983; *Sausen et al.*, 1995]. More recently, indices based upon the potential vorticity field have been developed [e.g., *Pelly and Hoskins*, 2003; *Schwierz et al.*, 2004], which have the advantage of being able to capture the dynamical features of the block.

[7] The potential vorticity (PV) based blocking detection algorithm is separated into two steps (see details given by *Schwierz et al.* [2004] and *Croci-Maspoli et al.* [2007]). First, regions of negative PV anomalies (< -1.3 pvu) between 500 hPa and 150 hPa are identified. These anoma-

[1]Max Planck Institute for Meteorology, Hamburg, Germany.
[2]Federal Office of Meteorology and Climatology MeteoSwiss, Zurich, Switzerland.

0094-8276/09/2009GL038259$05.00

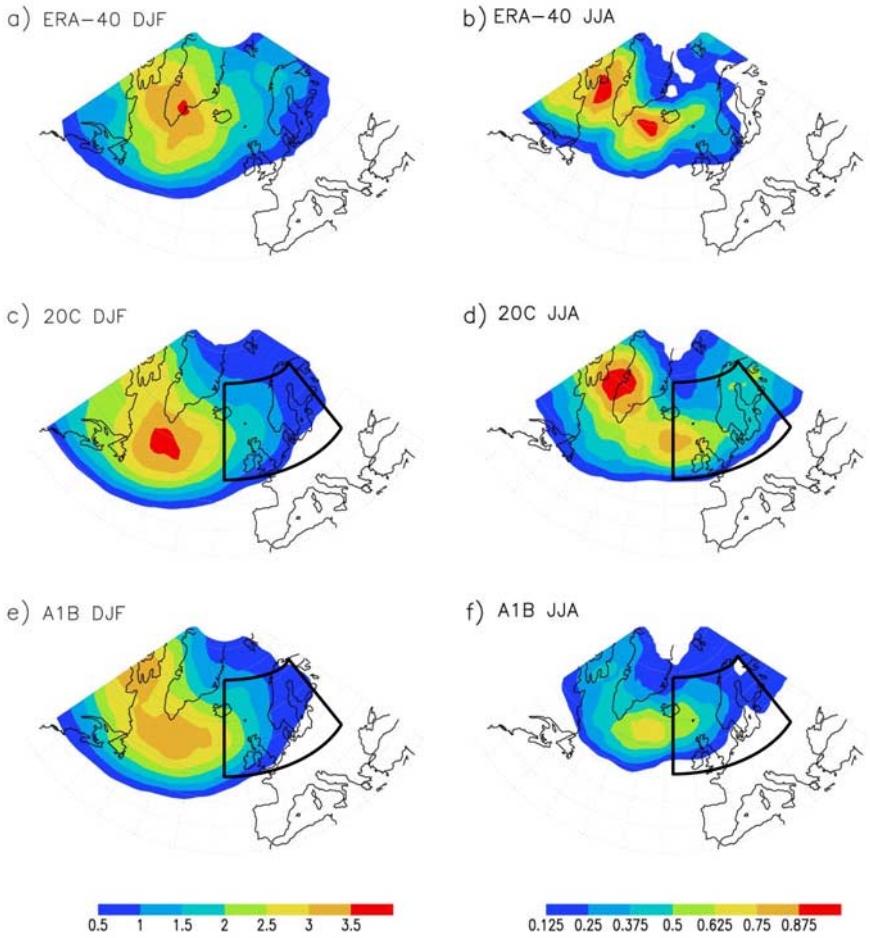

Figure 1. Climatologies of blocking frequency (%) for (left) winter (DJF) and (right) summer (JJA; note different scale). Shown are results for the present climate (1961–2000) in (a and b) ERA-40 and (c and d) ECHAM5 (ensemble means), and (e and f) for the A1B scenario (ensemble means 2160–2199). The black box frames blocking events in the EB region (15°W–30°E, 50°N–70°N), considered in the analysis.

lies are calculated with respect to the 1961–2000 and 2160–2199 periods, respectively. Second, these negative PV anomalies are temporally tracked (from genesis to lysis) and structures with a lifetime longer/equal than a specified time (here $\geq$ 10 days) are defined as blocking events. As a result, we obtain a two-dimensional blocking representation for every instant of time (6-hourly resolution).

[8] Due to the fact that we concentrate on the analysis of extreme events in Europe, we focus on blocks occurring close to Europe (15°W–30°E, 50°N–70°N) as depicted by the black box in Figure 1 (hereinafter referred to as European Blocks, EB).

2.3. Indices for Extreme Events

[9] In this study, extreme events are captured by monthly indices, such as maximum 5-day precipitation (RX5day), minimum of the minimum 2-m temperature (TNn) and maximum of the maximum 2-m temperature (TXx), as described by *Frich et al.* [2002]. These indices are widely used and characterize moderate but robust large-scale extreme events that are well captured by ECHAM5 [*Sillmann and Roeckner*, 2008]. RX5day is a useful indicator for large-scale flooding events. TXx and TNn represent the tails of the temperature distribution, corresponding to extreme day- and nighttime temperatures, respectively.

2.4. Composite Maps

[10] To depict the typical flow pattern as well as the typical temperature and precipitation fields associated with EB, we calculate composite maps for 6-hourly anomalies of 500 hPa geopotential height (Z500), 2m-temperature (TEMP2) as well as precipitation (PREC) for blocking events within the EB region. The statistical significance of the composite maps at the 1% significance level is established by the bootstrap resampling approach [*Efron and Tibshirani*, 1993].

2.5. Correlation Analysis

[11] We determine the associations between the blocking indicator and monthly indices for extreme events by calculating the Spearman's rank correlation coefficient. We test for correlations at the 5% significance level with a two-sided Spearman's rank correlation test according to *Best and Roberts* [1975]. With a field significance test [*Wilks*, 2006], which is conservative concerning spatial correlations, we further estimate the false discovery rate (FDR) of errone-

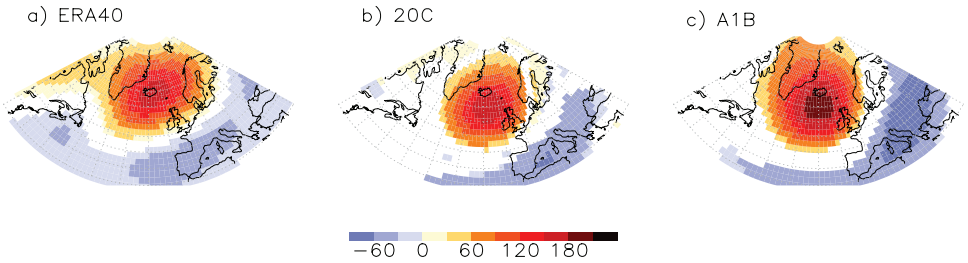

Figure 2. Composite maps of 6-hourly anomalies of Z500 [m] for EB averaged over DJF for (a) ERA-40 as well as the ensemble means of (b) 20C (1961–2000) and (c) A1B (2160–2199) simulations. Shown are only significant patterns to the 1% significance level.

ously rejected null hypothesis (no correlation) with a global test level of 5%.

[12] For the correlation analysis, the field average of blocking frequency over the EB region is calculated. We concatenated the respective 40-year time slices (1961–2000) and (2160–2199) of the three ensemble members, thus receiving time series of 120 years for the analysis of blocking frequencies and extreme indices in the 20C and A1B climate, respectively. Correlations between the EB blocking indicator and the extreme indices are then calculated at each grid point in the Euro-Atlantic domain. This approach enables us to include the model's internal climate variability into the correlation analysis.

3. Results

3.1. Blocking Climatology

[13] In Figure 1 climatologies of blocking frequencies are compared for the present (ERA-40 and 20C) and the future climate (A1B). Blocking frequencies are defined here as percentage of time a particular grid point is blocked by a block with a lifetime $\geq$ 10 days. Hence, a blocking frequency of 1%, for example, corresponds to about one blocked day per season. In general, there is good agreement between ECHAM5 and ERA-40 concerning the seasonal distribution and location of blocking. In the winter months, the location of highest blocking frequency in ERA-40 is found over southeastern Greenland. In ECHAM5 the center is shifted southward and is more extended than in ERA-40. Studies based on the Z500 anomaly fields [e.g., *Dole and Gordon*, 1983; *Bates and Meehl*, 1986; *Sausen et al.*, 1995] also found the winter maxima of blocking frequency to the southeast of Greenland. In contrast, studies based on the meridional Z500 gradient (e.g., TM90) find a maximum between the northern British Isles and Scandinavia (see *Scherrer et al.* [2006] for a discussion of these differences).

[14] In A1B, the DJF maximum blocking frequency decreases by about 15% relative to 20C and by about 8% on average in the EB region. The decrease around the southwestern part of Greenland and the increase in the western part of the EB region as seen in Figure 1e, has also been noticed in previous studies looking at trends in observations [e.g., *Croci-Maspoli et al.*, 2007]. Particularly in winter, there is a shift in blocking lifetime distribution towards longer blocks in future climate (not shown) in the EB region. For constant standard deviation the average blocking duration decreases for about 0.6 day in A1B compared to 20C. However, the maximum blocking duration of 12 days in 20C (and 11.5 days in ERA-40) increases to about 14 days in A1B.

[15] In summer (JJA) blockings are far less frequent than in winter. The area of high frequency in the Davies Strait is well captured, but the model underestimates the second maximum between Greenland and Iceland and overestimates the blocking frequency in the EB region. Summer blocking events experience a major decrease in A1B. The Davis Strait maximum disappears completely and the maximum is shifted southwest of Iceland. In the following, we exclude the summer because the correlations between the EB index and extreme events are statistically insignificant.

3.2. Composite Maps

[16] To get information about the impact of blocking on the mean climate, we illustrate the Z500 as well as the mean TEMP2 and PREC patterns associated with EB in winter for ERA-40 and model simulations. In present climate, positive Z500 anomalies (Figures 2a and 2b) centered between Iceland and the British Isles suggest northerly flow anomalies further east leading to an inflow of cold and dry air masses into Europe. In comparison to ERA-40, the model represents the Z500 anomalies very well with a slight southwestward shift of the positive Z500 anomaly center. In A1B, the positive Z500 anomalies intensify (30-40 hPa) around Iceland and expand further northward. Negative Z500 anomalies also intensify in southeastern Europe. This leads to an enforced north-south gradient of Z500 anomalies, thus stronger flow anomalies.

[17] The composite map of surface temperature (TEMP2, Figures 3a and 3b) shows pronounced cold anomalies (-3°C) in central Europe due to the northerly flow anomalies (e.g., T04). Positive anomalies (up to 4.4°C) over Greenland result from the southerly inflow of warm and humid air masses from the Atlantic. This pattern remains robust in A1B with even amplified positive and negative anomalies. The latter shifts towards eastern Europe, whereas the Iberian Peninsula does not show any negative anomalies in A1B.

[18] The composite map of precipitation in 20C (PREC, Figure 3c) depicts anomalously dry conditions around the British Isles where the mean winter precipitation is generally larger compared to other European regions (not shown). Positive anomalies can be found around the block, especially at the southeastern coast of Greenland. In A1B, the negative anomaly intensifies by -1 to -1.6 mm/d as well as the positive anomalies in Greenland and in the southern North Atlantic.

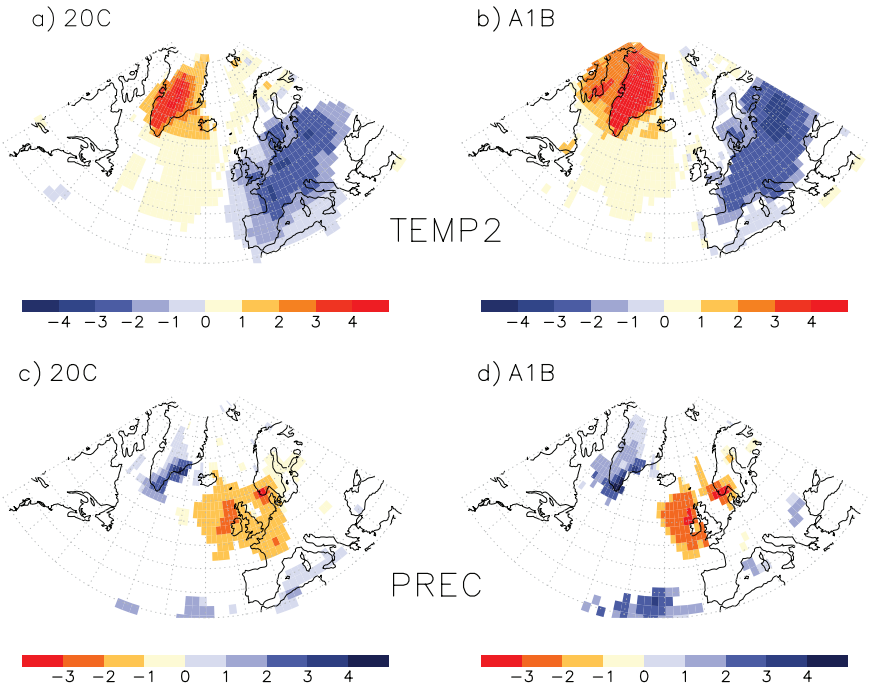

Figure 3. Composite maps of 6-hourly anomalies of (a and b) 2m-temperature [K] and (c and d) precipitation [mm/d] for EB averaged over DJF. Shown are the significant ensemble means at the 1% significance level for (left) 20C (1961–2000) and (right) A1B (2160–2199).

[19] The 20C composite maps of TEMP2 and PREC are similar to patterns received with ERA-40 (not shown), however the ERA-40 patterns are shifted northeastward similar to the Z500 composite map (Figure 2a). Furthermore, the composite maps of 20C resemble closely the patterns of Z500, temperature and precipitation as illustrated by T04 using NCEP/NCAR re-analysis data.

3.3. Correlation Analysis

[20] In Figure 4 we show associations between EB and selected temperature and precipitation extremes represented by monthly indices in 20C and A1B for DJF. In 20C, a coherent pattern of anti-correlation between EB and winter minimum temperature (TNn, Figures 4a and 4b) ranging from the Mediterranean Sea to northern Europe indicates very low nighttime temperatures in the presence of a block. In A1B, this pattern moves northeastward so that the Iberian Peninsula will be less affected by blocking episodes. The winter maximum temperature (TXx, Figures 4c and 4d) over Europe is largely uncorrelated with the EB index but significant positive correlations are found over Greenland, as already suggested by the positive temperature anomalies in the composite pattern. In A1B, the positive correlations over Greenland persist while negative correlations over Europe cover a larger area than in 20C and are extended northeastward, similar to the TNn pattern.

[21] The extreme precipitation index RX5day (Figures 4e and 4f) shows regions of positive correlation over Greenland and the North Atlantic, which bear some resemblance with the regions of positive anomalies in the composite maps. The Atlantic feature can be related to cyclonic systems at the southern flank of the block causing precipitation extremes in southern Europe. On the other hand, hardly any correlation is found in the core region where a coherent area of negative precipitation anomalies can be seen in the composite map. In A1B, more grid points showing anti-correlation appear over northern Europe, but still no coherent pattern emerges. The positive correlations over Greenland diminish, but the pattern over the North Atlantic spreads eastward, impacting the coast of Portugal and part of the Mediterranean area.

[22] The field significance test based on the FDR method reveals that the null hypothesis of no correlation can be rejected for all correlation patterns shown in Figure 4, indicating that the correlations obtained with the Spearman's rank test are not an artifact of the chosen local test level.

4. Concluding Remarks

[23] Using a dynamical PV-based blocking indicator we demonstrate that, compared to ERA-40, ECHAM5 simulates atmospheric blocking in the Euro-Atlantic region reasonably well with respect to location and frequency in both winter and summer. The composite patterns received with this blocking indicator are in striking resemblance to the respective composites by T04 generated with a Z500-based blocking indicator. In comparison to the latter, the PV-based blocking indicator is able to capture the block in each state of its life cycle [*Croci-Maspoli et al.*, 2007]. Thus, also the impact of blocking events occurring in the western North Atlantic (major blocking genesis region) could be studied, which is relevant for the North American continent.

[24] There are some distinct differences between the 6-hourly composite maps and the monthly correlation patters, caused mainly by the different temporal resolution. The composite map of TEMP2 summarizes both effects of

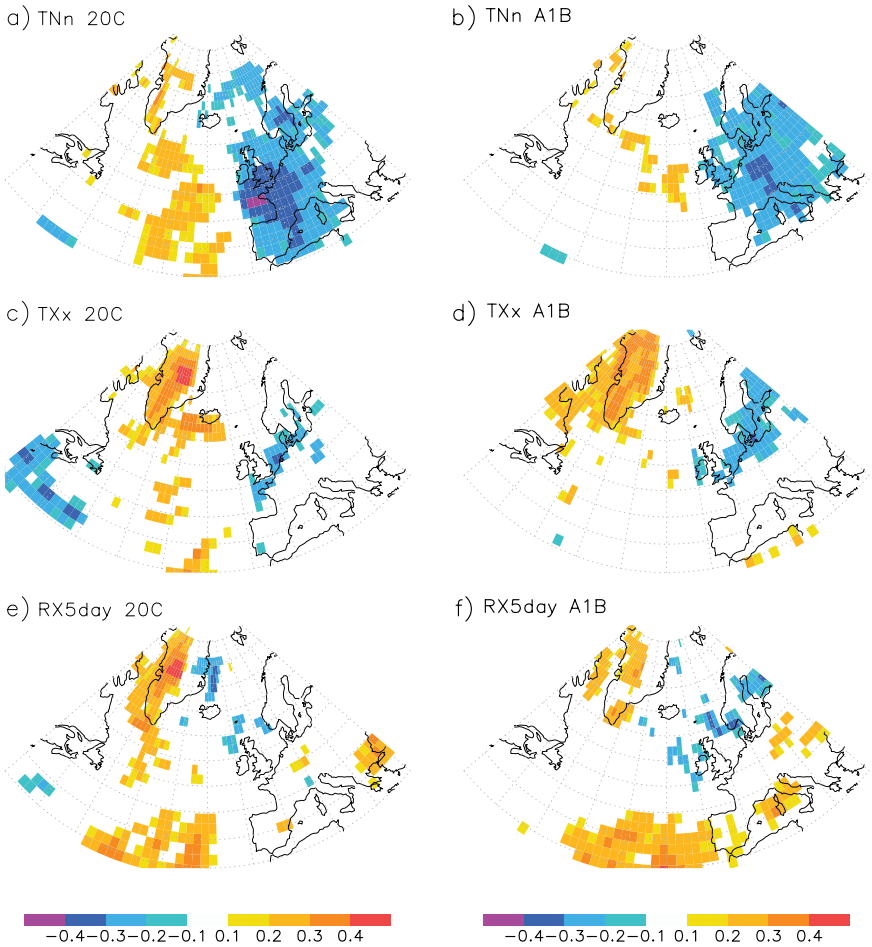

Figure 4. Spearman's rank correlation coefficients showing significant correlations at the 5% level for winter between the field average of blocking frequency over the EB region and extreme indices (a and b) TNn, (c and d) TXx and (e and f) RX5day. (left) 20C (1961–2000); (right) A1B (2160–2199).

EB on monthly extreme minimum and maximum temperatures. Negative anomalies of TEMP2 in large parts of Europe are mainly caused by northerly flow anomalies to the east of the blocking core region [*Rex*, 1951]. The enhanced nighttime radiative cooling due to reduced humidity and cloudiness in the presence of blocking (T04) has an effect especially on the extreme winter minimum temperature. This is not reflected in the extreme winter maximum temperature showing hardly any correlation in Europe. This indicates that EB, even though their lifetime is less than a month, have a sustained influence especially on the extreme winter minimum temperature.

[25] In the A1B scenario, the decreasing blocking frequency and increase in maximum blocking duration result in a shift and intensification of the associated Z500 anomaly around the British Islands towards the Norwegian Sea. Due to a northeastward shift of the blocking pattern in the EB region, a larger part of Europe is affected by anomalously cold winter months. Compared to 20C, the correlation patterns generally weaken in magnitude being more sensitive to the reduced number of blocks. On the other hand, composite patterns of TEMP2 and PREC are amplified in A1B due to increase in maximum blocking duration in the EB region.

[26] Thus, in a warmer climate blocking events tend to moderate temperature and precipitation changes (as described by, e.g., *Sillmann and Roeckner* [2008]). However, we should note that atmospheric blocking only explains some 14% [cf. *Scherrer et al.*, 2006] of the European climate variability and other regimes such as the North Atlantic Oscillation have to be considered in this context as well.

[27] **Acknowledgments.** We thank Erich Roeckner and three anonymous reviewers for their helpful comments and suggestions. We acknowledge Rick Katz and Korbinian Strimmer for their advises on the test statistic. Further we thank ECMWF and MeteoSwiss for providing access to ERA-40 data. The project was partly supported by the Swiss NCCR Climate Program and the IMPRS for Earth System Modelling.

References

Bates, G., and G. A. Meehl (1986), The effect of CO_2 concentration on the frequency of blocking in a general circulation model coupled to a simple mixed layer ocean, *Mon. Weather Rev.*, *114*, 687–701.

Best, D. J., and D. E. Roberts (1975), Algorithm AS 89: The upper tail probabilities of Spearman's rho, *Appl. Stat.*, *24*, 377–379.

Croci-Maspoli, M., C. Schwierz, and H. C. Davies (2007), A multifaced climatology of atmospheric blocking and its recent linear trend, *J. Clim.*, *20*, 633–649.

D'Andrea, F., et al. (1998), Northern Hemisphere atmospheric blocking as simulated by 15 atmospheric general circulation models in the period 1979–1988, *Clim. Dyn.*, *14*, 385–407.

Doblas-Reyes, F. J., M. J. Casado, and M. A. Pastor (2002), Sensitivity of the Northern Hemisphere blocking frequency to the detection index, *J. Geophys. Res.*, *107*(D2), 4009, doi:10.1029/2000JD000290.

Dole, R. M., and N. D. Gordon (1983), Persistent anomalies of the extratropical Northern Hemisphere wintertime circulation: Geographical distribution and regional persistence characteristics, *Mon. Weather Rev.*, *111*, 1567–1586.

Efron, B., and R. J. Tibshirani (1993), *An Introduction to the Bootstrap*, *Monogr. Stat. Appl. Probab.*, vol. 57, 456 pp., Chapman and Hall, New York.

Frich, P., L. V. Alexander, P. Della-Marta, B. Gleason, M. Haylock, A. M. Klein Tank, and T. Peterson (2002), Observed coherent changes in climate extremes during the second half of the twentieth century, *Clim. Res.*, *19*, 193–212.

Jungclaus, J. H., M. Botzet, H. Haak, N. Keenlyside, J.-J. Luo, M. Latif, J. Marotzke, U. Mikolajewicz, and E. Roeckner (2006), Ocean circulation and tropical variability in the coupled model ECHAM5/MPI-OM, *J. Clim.*, *19*, 3952–3972.

Pelly, J. L., and B. J. Hoskins (2003), How well does the ECMWF Ensemble prediction system predict blocking?, *Q. J. R. Meteorol. Soc.*, *129*, 1683–1702.

Rex, D. F. (1951), The effect of Atlantic blocking action upon European climate, *Tellus*, *3*, 1–16.

Sausen, R., W. Koenig, and F. Sielmann (1995), Analysis of blocking events from observations and ECHAM model simulations, *Tellus, Ser. A*, *47*, 421–438.

Scherrer, S. C., M. Croci-Maspoli, C. Schwierz, and C. Appenzeller (2006), Two-dimensional indices of atmospheric blocking and their statistical relationship with winter climate patterns in the Euro-Atlantic region, *Int. J. Climatol.*, *26*, 233–249.

Schwierz, C., M. Croci-Maspoli, and H. C. Davies (2004), Perspicacious indicators of atmospheric blocking, *Geophys. Res. Lett.*, *31*, L06125, doi:10.1029/2003GL019341.

Sillmann, J., and E. Roeckner (2008), Indices for extreme climate events in projections of anthropogenic climate change, *Clim. Change*, *86*, 83–104.

Tibaldi, S., and F. Molteni (1990), On the operational predictability of blocking, *Tellus, Ser. A*, *42*, 343–365.

Trigo, R., I. Trigo, C. DaCamara, and T. J. Osborn (2004), Climate impact of the European winter blocking episodes from the NCEP/NCAR Reanalysis, *Clim. Dyn.*, *23*, 17–28.

Uppala, S. M., et al. (2005), The ERA-40 re-analysis, *Q. J. R. Meteorol. Soc.*, *131*, 2961–3012.

Wilks, D. S. (2006), On "field significance" and the false discovery rate, *J. Appl. Meteorol. Climatol.*, *45*, 1181–1189.

M. Croci-Maspoli, Federal Office of Meteorology and Climatology MeteoSwiss, Kraehbuehlstrasse 58, CH-8044 Zurich, Switzerland.

J. Sillmann, Max Planck Institute for Meteorology, Bundesstrasse 53, D-20146 Hamburg, Germany. (jana.sillmann@zmaw.de)